Optimization Of Underground Mine Communication with Millimetre-Wave Massive MU-MIMO

M. NAVYA SREE[1], C. SHIVANI[2], B. LAXMI PRIYA[3], L.V.R. CHAITANYA PRASAD[4]
[1, 2, 3, 4]*Department of ECE, Sreenidhi Institute of Science and Technology, Hyderabad, India*

Abstract- ***This paper investigates the performance of a large multiuser multiple-input multiple-output (MU-MIMO) millimeter-wave (mmWave) communication system deployed in an underground mining environment. The study is based on empirical channel measurements conducted at 28 GHz using a base station equipped with 256 virtual antenna elements. Key channel parameters such as path loss, RMS delay spread, coherence bandwidth, and sum-rate capacity are analyzed. Results show that a multislope path loss model offers better accuracy than traditional models. The findings demonstrate the potential of massive MIMO in harsh underground environments for 5G and beyond.***

Index Terms—MU-MIMO, mmWave, underground mine, channel capacity, path loss, delay spread

I. INTRODUCTION

Underground mine communication is a critical challenge for automation, safety, and operational efficiency. Unlike above- ground environments, underground mines present a highly complex and dynamic wireless propagation environment characterized by narrow tunnels, irregular geometries, high humidity, and metallic infrastructure. These conditions result in severe multipath propagation, signal blockages, diffraction, and attenuation, which degrade the performance of traditional narrowband radio systems and make reliable communication difficult. Additionally, signal penetration through rock and soil is minimal, limiting the effectiveness of conventional wireless solutions.

To address these issues, the adoption of fifth-generation (5G) wireless technologies, particularly millimeter-wave (mmWave) frequencies combined with massive Multiple-Input Multiple-Output (MIMO) systems, offers significant promise. mmWave frequencies provide large bandwidths, enabling ultra-high data rates required for real-time monitoring, video surveillance, and control of autonomous mining equipment. However, mmWave signals are inherently susceptible to high path loss and require advanced beamforming techniques to maintain link reliability.

II. LITERATURE REVIEW

Reconfigurable Intelligent Surfaces (RIS), advanced beam- forming, and hidden Markov model (HMM)-based PLC systems have been explored to address wireless communication challenges in underground tunnels. RIS offers a low-power method to enhance signal coverage by intelligently reflecting signals toward desired directions, reducing the need for additional infrastructure [1].

Beamforming in massive MIMO systems allows precise signal focusing, improving SNR and reducing interference—particularly valuable in mines where reflections and obstructions are common. Techniques like zero-forcing and block diagonalization have shown promise in managing user separation and enhancing spectral efficiency [2].

HMM-based PLC models account for the non-stationary nature of underground environments, helping predict errors due to machinery movement and varying channel conditions [3]. Furthermore, studies at 28 GHz and 60 GHz confirm that tunnel curvature, surface roughness, and metallic structures significantly influence path loss and delay spread, emphasizing the need for frequency- and geometry-specific modeling [4].

A. Existing Method Overview

To evaluate mmWave massive MU-MIMO performance in underground environments, a baseline

system using a 64- element virtual Uniform Rectangular Array (URA) was deployed. Channel measurements were conducted at 28 GHz using frequency-domain channel sounding, aligning with 3GPP band n257 (27.5–28.35 GHz), a priority band for mmWave systems in Canada and the USA. Despite its significance, this band remains largely unexplored in subterranean settings.

1) Measurement Environment: The campaign was carried out in the Old Lamaque gold mine in Val-d'Or, Quebec, Canada. Measurements were taken inside a gallery located 91 meters underground. The tunnel, with an average width of 3.8 meters and height of 2.8 meters, includes curved sections, a 20% downward slope, and high humidity (up to 100%). Its rough, metallic-lined surfaces and structural reinforcements (bolts and nets) introduce significant scattering.
2) System Setup and Configuration:

- Transmit Power and Bandwidth: RF transmit power was fixed at 6 dBm with 800 MHz bandwidth.
- Sweeps and Delay Spread: 1201 sweep points enabled measurement of excess delays up to 1.5 μs.
- Receiver (BS) Configuration: A virtual URA of 64 antennas was emulated using a movable horn antenna spaced at λ/2, mounted 1.7 m high near the gallery wall.
- Transmitter (UE) Configuration: A horn antenna on a 1.6 m tripod was used to emulate user equipment (UE) across 17 predefined locations—12 LOS and 5 NLOS.
- Antenna Alignment: Laser beam alignment ensured accurate pointing to the center of the URA at each Tx point.
- Calibration: The VNA was calibrated using the Short- Open-Load-Thru (SOLT) method to eliminate cable and passive component effects.

At each Tx-Rx location, both the Channel Transfer Function (CTF) and Channel Impulse Response (CIR) were recorded, yielding 2176 total measurements.

3) *Reference and Calibration Equations:*

$$H(f) = \frac{H_{21}(f)}{H_{sys}(f)} \quad (1)$$

$$H_{sys}(f) = \frac{H_{21ref}(f)}{H_{ref}(f)} \quad (2)$$

Reference measurements were taken at 1 m in an anechoic chamber to quantify system imperfections (e.g., RFoF link, fiber, amplifiers).

4) Path Loss Calculation and Modeling: Path loss was calculated as:

$$PL(f) = -10 \log_{10}\left(\frac{1}{N}\sum_{n=1}^{N} |H(f_n)|^2\right) \quad (3)$$

After calibration, the wideband path loss was expressed as:

$$PL(f) = -10 \log_{10}\left(\frac{1}{N}\sum_{n=1}^{N} |H(f_n)|^2\right) \quad (3)$$

After calibration, the wideband path loss was expressed as:

$$PL_{WB} = -10 \log_{10}\left(\sum_{n=1}^{N} |H(f_n)|^2\right) \quad (4)$$

The log-distance model was used for path loss modeling:

$$PL(d) = PL(d_0) + 10n \log_{10}(d/d_0) + \chi_\sigma \quad (5)$$

where n is the path loss exponent and χ_σ is a Gaussian random variable representing shadowing effects.

5) Limitations of the Existing Setup:

High Bit Error Rate (BER): Despite theoretical benefits of massive MIMO, high BER was observed—especially under NLOS conditions—due to severe multipath, scattering and poor channel estimation.

Limited Throughput and Capacity: Several factors hindered performance:

– Constrained spatial degrees of freedom due to tunnel geometry.
– High mmWave attenuation and poor obstacle penetration at 28 GHz.
– Increased delay spread and interference in NLOS regions.
– Practical limitations such as antenna misalignment and calibration drift.

III. PROPOSED METHOD

To overcome these limitations, a 256-antenna massive MIMO base station is proposed. With increased spatial degrees of freedom, this setup supports enhanced beamforming, user separation, and SNR.

A. Measurement Setup

The system used a 16×16 URA with λ/2 spacing. Calibration was performed using the Short-Open-Load-Thru (SOLT) technique. Measurements covered multiple Tx locations and tunnel configurations, improving angular resolution and spatial diversity.

B. Multislope Path Loss Model

The proposed model segments the propagation environment into zones with distinct path loss exponents:

$$PL(d) = PL_0 + 10n_1 \log_{10}(d/d_0) + X_\sigma, \quad d < d_{bp} \quad (6)$$

$$PL(d) = PL_1 + 10n_2 \log_{10}(d/d_{bp}) + X_\sigma, \quad d \geq d_{bp} \quad (7)$$

where Xσ is a zero-mean Gaussian random variable modelling shadow fading.

C. Channel Transfer Function

Channel behavior is characterized using frequency-domain measurements. The calibrated channel transfer function (CTF) is given by:

$$H(f) = \frac{H_{21}(f)}{\overline{H_{sys}(f)}} \quad (8)$$

D. Path Loss Calculation

Wideband path loss is extracted by averaging the squared magnitude of the calibrated CTF:

E. Performance Metrics

1) RMS Delay Spread: RMS delay spread (τ_{rms}) measures the time dispersion due to multipath. Lower values correspond to reduced inter-symbol interference and improved channel quality.

2) Channel Capacity: Channel capacity is calculated using Shannon's formula:

$$C = B \log_2\left(1 + \frac{P_r}{N_0 B}\right) \quad (10)$$

where B is the bandwidth, P_r is the received power, and N_0 is the noise power spectral density. The 256-antenna array enhances Pr through precise beamforming, leading to improved capacity and support for high-throughput applications.

IV. RESULTS AND DISCUSSION

A. Delay Spread

Analysis revealed that 90% of measured RMS delay spreads were below 4 ns, indicating minimal temporal dispersion and excellent channel conditions. This is critical in maintaining low inter-symbol interference (ISI), especially for high data rate applications. The delay spread was observed to be largely independent of Tx-Rx separation, suggesting uniform scattering behavior due to the waveguide-like structure of the tunnels.

B. Capacity Analysis

System capacity was evaluated using Shannon's capacity formula:

$$C = B \cdot \log2(1 + SNR) \quad (11)$$

For a configuration using 256 antennas and 8 users, the system achieved a peak spectral efficiency of 33.54 bits/s/Hz. This demonstrates the high potential of massive MIMO for dense underground deployments. However, as the number of simultaneously served users increases, inter-user interference rises, leading to reduced capacity per user. This trade-off high- lights the importance of advanced scheduling and precoding strategies in high-user scenarios.

C. Figures

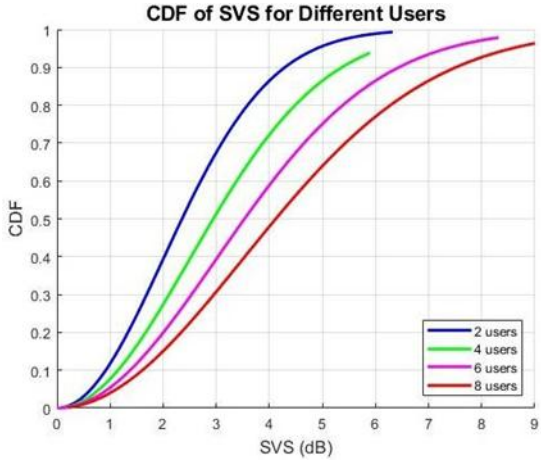

Fig. 1: CDF of SVS for Different Users

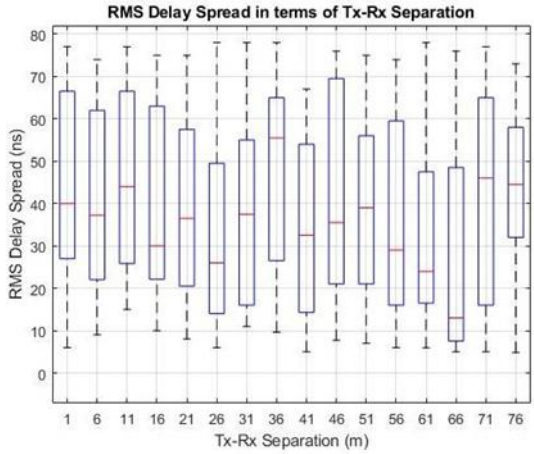

Fig. 2: Distribution of RMS delay spread over different Tx-Rx distances

V. APPLICATIONS

The high capacity, low delay spread, and robust channel behavior offered by the 256-antenna massive MIMO system enable a range of critical applications in underground mining and tunnel environments:

- Autonomous Mining Vehicles: Reliable communication for navigation, obstacle detection, and remote control.
- Real-Time Sensor Networks: High-bandwidth support for dense sensor deployments monitoring gas levels, vibrations, and equipment health.
- Wireless Control of Excavation Tools: Low-latency links facilitate precision control and increased safety for remotely operated machinery.
- Enhanced Voice and Video Communication: Clear, un- interrupted communication for operational coordination and emergency response.
- Predictive Maintenance Systems: Continuous data flow from connected assets enables real-time analytics and fault prediction.

CONCLUSION

This research highlights the potential of massive MU-MIMO technology operating at 28 GHz to transform wireless communication in underground mining environments. The deployment of a 256-element antenna array enables high- resolution beamforming and robust spatial multiplexing, both of which are essential for maintaining link quality in harsh, non-line-of-sight (NLOS) scenarios where traditional systems struggle.

Through comprehensive frequency-domain channel sounding and detailed measurement campaigns in realistic tunnel configurations, the study captured critical parameters such as path loss, delay spread, and system capacity. The refined multislope path loss model accurately reflects the propagation characteristics in underground spaces, taking into account waveguide effects, breakpoints, and deep NLOS attenuation.

Results indicate that 90% of delay spreads remained under 4 ns, ensuring low temporal dispersion and minimal inter- symbol interference. Furthermore, system capacity scaled with antenna count, achieving up to 33.54 bits/s/Hz with eight users. These results underscore the suitability of massive MIMO for supporting bandwidth-intensive applications such as real- time video surveillance, autonomous equipment operation, and dense IoT sensor networks in subterranean settings.

The outcomes of this work provide a foundational frame- work for implementing 5G-enabled private networks in mines. By improving spectral efficiency, reliability, and system scalability, the proposed approach offers a significant leap toward intelligent, automated, and safer mining operations. The in- sights gained also contribute to the broader field of mmWave communication in constrained and complex environments.

REFERENCES

[1] J. Lo¨o¨w, L. Abrahamsson, and J. Johansson, "Mining 4.0—The impact of new technology from a work place perspective," Mining, Metall. Ex- ploration, vol. 36, no. 4, pp. 701–707, Aug. 2019, doi: 10.1007/s42461-019-00104-9.

[2] S. M. Riurean, M. Leba, and A. C. Ionica, "Conventional and advanced technologies for wireless transmission in underground mines," in Appli- cation of Visible Light Wireless Communication in Underground Mine. Cham, Switzerland: Springer, 2021, pp. 41–125.

[3] M. Jadoul. (2021). Here is Why Mining is Digging Into 5G. [Blog] NOKIA. [Online]. Available: https://www.nokia.com/blog/here- is-whymining-is-digging-into-5g/

[4] M. Ghaddar, I. Ben Mabrouk, M. Nedil, K. Hettak, and L. Talbi, "Deterministic modeling of 5G millimeter-wave communication in an underground mine tunnel," IEEE Access, vol. 7, pp. 116519–116528, 2019.

[5] O. Kolade and L. Cheng, "Markov model characterization of a multi- carrier narrowband powerline channel with memory in an underground mining environment," IEEE Access, vol. 9, pp. 59085–59092, 2021.

[6] R. Flamini et al., "Toward a heterogeneous smart electromagnetic environment for millimeter-wave communications: An industrial view-point," IEEE Trans. Antennas Propag., vol. 70, no. 10, pp. 8898–8910, Oct. 2022.

[7] T. S. Rappaport, G. R. MacCartney, M. K. Samimi, and S. Sun, "Wideband millimeter wave propagation measurements and channel models for future wireless communication system design," IEEE Trans. Commun., vol. 63, no. 9, pp. 3029–3056, Sep. 2015.

[8] R. Maccartney, T. S. Rappaport, S. Sun, and S. Deng, "Indoor office wideband millimeter-wave propagation measurements and channel models at 28 and 73 GHz for ultra dense 5G wireless networks," IEEE Access, vol. 3, pp. 2388–2424, 2015.

[9] J.-Y. Lee, J.-H. Lee, and S.-C. Kim, "Improving the accuracy of millimeter-wave ray tracing simulations by modeling roadside trees," IEEE Antennas Wireless Propag. Lett., vol. 18, no. 1, pp. 162–166, Jan. 2019.

[10] X. Gao, O. Edfors, F. Rusek, and F. Tufvesson, "Massive MIMO performance evaluation based on measured propagation data," IEEE Trans. Wireless Commun., vol. 14, no. 7, pp. 3899–3911, Jul. 2015.

[11] S. Mumtaz, J. Rodriguez, and L. Dai, "mmWave Massive MIMO: A Paradigm for 5G. New York, NY, USA: Academic, 2016.

[12] J. Huang, C.-X. Wang, R. Feng, J. Sun, W. Zhang, and Y. Yang, "Multi-frequency mmWave massive MIMO channel measurements and characterization for 5G wireless communication systems," IEEE J. Sel. Areas Commun., vol. 35, no. 7, pp. 1591–1605, Jul. 2017.

[13] M. Shafi et al., "5G: A tutorial overview of standards, trials, challenges, deployment, and practice," IEEE J. Sel. Areas Commun., vol. 35, no. 6, pp. 1201–1221, Jun. 2017.

[14] S. A. M. Tariq, C. L. Despins, S. Affes, and C. Nerguizian, "Angular dispersion of a scattered underground wireless channel at 60 GHz," IEEE Access, vol. 8, pp. 67572–67580, 2020.

[15] Wang, W. Ji, G. Zheng, and A. Saleem, "Analysis of propagation characteristics for various subway tunnel scenarios at 28 GHz," Int. J. Antennas Propag., vol. 2021, pp. 1–16, Sep. 2021.

[16] Rusek, D. H. T. Nguyen, B. M. Sadler, and L. E. Frenger, "Scaling up MIMO: The power of massive MIMO," IEEE Signal Processing Mag., vol. 30, no. 1, pp. 40–60, Jan. 2013.

[17] Goldsmith, "Wireless Communications," Cambridge University Press, 2005.

[18] A. Alkhateeb, J. Mo, N. Gonzalez-Prelcic, and R. W. Heath Jr., "Channel estimation and hybrid precoding for millimeter wave cellular systems," IEEE J. Sel. Topics Signal Process., vol. 8, no. 5, pp. 5–18, Oct. 2014.